

The elusive structure of the diffuse molecular gas: shocks or vortices in compressible turbulence?

J. Pety and É. Falgarone

Radioastronomie, CNRS, UMR 8540, École Normale Supérieure, 24 rue Lhomond, F-75005 Paris, France

Received xxxx / Accepted xxxx

Abstract. The cold diffuse interstellar medium must harbor pockets of hot gas to produce the large observed abundances of molecular species, the formation of which require much more energy than available in the bulk of its volume. These hot spots have so far escaped direct detection but observations and modeling severely constrain their phase-space structure i.e. they must have a small volume filling factor (a few %), surface filling factors larger than unity with large fluctuations about average and comparable velocity structure in “pencil beams” and “large beams”.

The dissipation of the non-thermal energy of supersonic turbulence occurs in bursts, either in shocks or in the regions of large shear at the boundary of coherent vortices. These two processes are susceptible to generate localized hot regions in the cold medium. Yet, it is of interest to determine which of them, if any, dominates the dissipation of turbulence in the cold interstellar medium.

In this paper, we analyze the spatial and kinematic properties of two subsets of hydrodynamical compressible turbulence: the regions of largest negative divergence and those of largest vorticity and confront them with the observational constraints. We find that these two subsets fulfill the constraints equally well. A similar analysis should be conducted in the future on simulations of MHD turbulence.

Key words: ISM: evolution - ISM: kinematics and dynamics - ISM: molecules - ISM: structure - Turbulence

1. Introduction

For several decades now, molecules have been detected in the diffuse component of the cold neutral medium and these observations raise several intriguing questions. Firstly, the large observed abundances of CH^+ (Crane et al., 1995; Grede, 1997) and HCO^+ and OH (Lucas and Liszt, 1996) in the cold diffuse medium imply that activation barriers and endothermicities of several thousands Kelvin be overcome. The formation of CH^+ proceeds through the endothermic reaction of C^+ with H_2 ($\Delta E/k=4640$ K) and that of OH via the reaction of O with

H_2 which has an activation energy $\Delta E/k=2980$ K. In the diffuse gas, HCO^+ forms from CH_3^+ , a daughter molecule of CH^+ . None of the large observed abundances can be explained by standard steady-state chemistry in cold diffuse gas. Pockets of hot gas must therefore exist in the cold diffuse medium.

Secondly, many other molecules like CO, CS, SO, CN, HCN, HNC, H_2S , C_2H have now been detected in absorption in front of extragalactic continuum sources in local or redshifted gas (Lucas & Liszt 1993, 1994, 1997; Liszt & Lucas 1994, 1995, 1996; Wiklind & Combes 1997, 1998). The lines of sight sample the edges of molecular clouds or the diffuse medium, which corresponds to gas poorly shielded from the ambient UV radiation field. This derives from the low excitation temperatures (often close to the temperature of the cosmic background) measured in these transitions. Yet, the molecular abundances derived are close to those of dark clouds.

Thirdly, the spatial and velocity distribution of these molecules is highly elusive. Observations of CO emission and absorption lines toward extragalactic sources by Liszt & Lucas (1998) show that: (i) absorption and emission line profiles have comparable linewidths whereas the projected size of the sampled volumes of gas differ by more than four orders of magnitude (60 vs. 10^{-3} arcsec), (ii) the excitation temperature of the CO molecules changes only weakly across the profiles and (iii) there are very few lines of sight with no absorption line detected. The phase-space distribution of the CO-rich gas in diffuse clouds must therefore have a surface filling factor close to unity, and its velocity field must be as adequately sampled by a pencil beam than by a large beam. As mentioned by the authors, these observations suggest a one-dimensional structure for the molecular component, which contrasts with the profuse small scale structure observed in emission.

Two mechanisms, operating at very different size scales, can trigger a *hot chemistry* in the cold diffuse medium and produce the observed molecular abundances: magneto-hydrodynamical (MHD) shocks (Elitzur and Watson, 1978; Draine and Katz, 1986; Draine, 1986; Pineau des Forts et al., 1986; Flower and Pineau des Forts, 1998) and intense coherent vortices, responsible for a non-negligible fraction of the viscous dissipation of supersonic turbulence (Falgarone and Puget, 1995; Falgarone et al., 1995; Joulain et al., 1998). This is so because the dissipation of the non-thermal energy of super-

Send offprint requests to: J. Pety

Correspondence to: pety@lra.ens.fr

sonic turbulence is concentrated in shocks and in the regions of large shear at the boundary of coherent vortices. In both cases, only a few % of hot gas on any line of sight across the cold medium is sufficient to reproduce the observed column densities of molecules. This small fraction of hot gas corresponds to about 6 MHD shocks of 10 km s^{-1} or 1000 vortices with rotation velocity of 3.5 km s^{-1} per magnitude of gas (or $N_{\text{tot}} = 1.8 \times 10^{21} \text{ cm}^{-2}$) of density $n \approx 30 \text{ cm}^{-3}$ (Verstraete et al., 1999).

The main problem met with the models of individual C shocks or vortices is that the predicted shift between neutral and ionized species is larger than observed. In this paper, we simply address the issue of the impact of the line of sight averaging upon the resulting line profiles in a turbulent velocity field. We investigate the spatial and velocity distribution of the regions of high vorticity or high negative divergence (shocks) in a simulation of compressible turbulence to test whether or not the space-velocity characteristics of any of these subsets fulfill the observational requirements. We carry our analysis on the numerical simulations of compressible turbulence of Porter, Pouquet & Woodward (1994). They are 512^3 simulations of mildly compressible turbulence (initial rms Mach number=1). The time step analysed here is $t = 1.2\tau_{\text{ac}}$ where τ_{ac} is the acoustic crossing time. At that epoch in the simulation, many shocks have survived producing density contrasts as large as 40, but the bulk of the energy at small scales is contained in the vortical modes.

These simulations are hydrodynamical and do not include magnetic field. The impact of magnetic field upon the statistical properties of turbulence may be less important than foreseen. Recent simulations of MHD compressible turbulence (Ostriker et al., 1999) show that the dissipation timescale of MHD turbulence is closer than previously thought to that of hydrodynamical turbulence. Descriptions of the energy cascade in models of MHD turbulence also predict that vortices must play an important role (Goldreich and Sridhar, 1995; Lazarian and Vishniac, 1999). Magnetic field does not prevent either the intermittency of the velocity field to develop (Brandenburg et al., 1996; Galtier et al., 1998; Politano and Pouquet, 1998b; Politano and Pouquet, 1998a; Politano and Pouquet, 1995). In MHD as in hydrodynamic turbulence, shocks interact and generate vortex layers, which are Kelvin-Helmholtz unstable and eventually form vorticity filaments.

Another limitation of our study lies in the fact that the Reynolds number of the simulations is small compared to that of interstellar turbulence. Recent studies of high Reynolds number turbulence in Helium bring the unexpected result that the statistical properties of the velocity field have little dependence with the Reynolds number, at large Reynolds numbers (Tabeling et al., 1996). We therefore believe that the analysis presented here on hydrodynamical simulations has some relevance to the understanding of interstellar turbulence.

We discuss the velocity structure of the two subsets (regions of high vorticity or of high negative divergence) and compare in each case the velocity samplings provided by pencil beams versus large beams (Sect. 2). In Sect. 3, we discuss the spa-

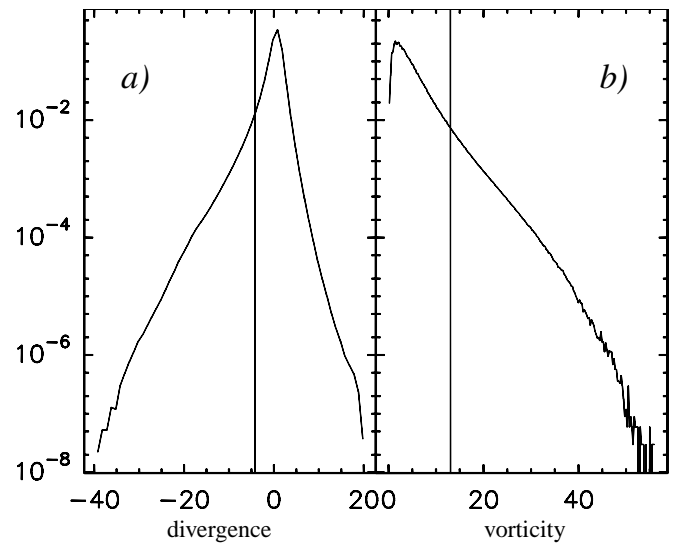


Fig. 1. PDFs of the values of (a) the positive and negative divergence and (b) the vorticity in the whole cube. The integrated numbers of points below (case a) above (case b) each threshold indicated by a vertical bar are 3%.

tial distributions of the two subsets. In Sect. 4, we compare the results derived from the numerical simulations with the observations.

2. Velocity structure of subsets of intense vortices and shocks in compressible turbulence.

2.1. Integrated profiles

We first compare the velocity distributions obtained with all the data points in the simulation with those obtained by selecting only 3% (or 4×10^6) of these data points. These subsamples are of three kinds: a subset of randomly selected positions in space and the upper tails of the distributions of the negative divergence and vorticity (see Figs. 1a and 1b). In the following, for the sake of simplicity, we will call them shocks and vortices.

The choice of 3% of the points is a compromise between the value of $\approx 1\%$ dictated by the chemical models and their confrontation to the observations and a number large enough so that the statistical analysis described below be meaningful. The actual values of the thresholds in the vorticity or in the divergence correspond to this choice. As said above, many of the molecular species observed in the cold diffuse medium, require large temperatures for their formation. Below gas temperatures of the order of 10^3 K , there is an exponential cut-off of the speed or the probability of these chemical reactions. Since the heating sources are either the viscous dissipation enhanced in the layers of large velocity shear at the boundary of coherent vortices (Joulain et al., 1998), or the ion-neutral streaming in the magnetic precursor of the shocks (Flower and Pineau des Forts, 1995), the thresholds in vorticity and in negative divergence correspond to temperature thresholds. It is only above such thresholds in negative divergence (shock velocity) or vorticity (shear), that the *hot chemistry* required by the observa-

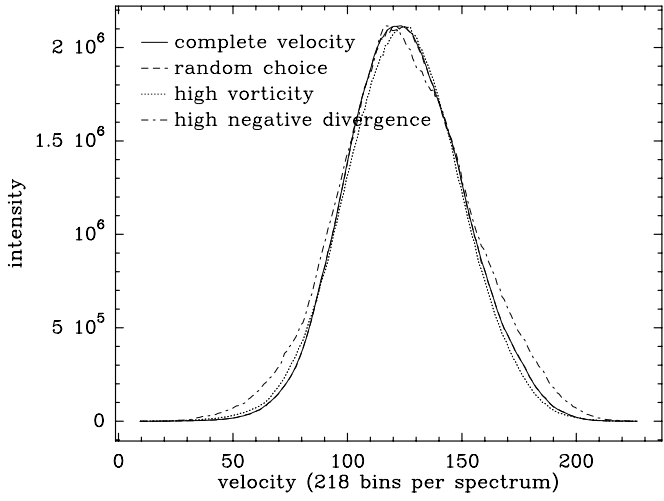


Fig. 2. Velocity distributions obtained with the full velocity field and all the points in the simulation (solid), with 3% of the data points randomly selected in space (dashed), with the 3% of the points which have the largest vorticity (dotted) and with the 3% of the points which have the largest negative divergence (dot-dashed). The intensity scale corresponds to the number of points in each of the 218 velocity bins. The velocity scale is the bin number.

tions can be triggered in the cold diffuse medium. As seen on Fig. 1, the selected thresholds for the vorticity and the divergence fall in the non-Maxwellian (non-Gaussian) tails of each distribution. The sets of structures that we describe therefore belong to the non-Maxwellian (non-Gaussian) tails of the corresponding distributions.

The velocity distributions of each subset (normalized to their peak value) is shown in Fig. 2 together with that of the whole cube. They are remarkably similar. The only subset which provides a slightly (10%) broader spectrum is that built on the shocks. A tracer passively advected in a turbulent flow (subset of spatially random positions) would therefore carry the characteristics of the turbulent field of the bulk of the volume, even though its volume filling factor is as small as a few %.

2.2. Velocity widths of pencil beam and large beam line profiles.

We now compare the velocity width of synthetic spectra obtained with a large beam (i.e. profiles observed in emission) to those obtained in a pencil beam (i.e. profiles observed in absorption). To do so we have computed the velocity distribution in $4 \times 4 \times 512$ subsamples of the whole cube and of the two subsets of largest vorticity and largest divergence. Under the approximation that the line radiation is optically thin (Falgarone et al., 1994), we consider that these velocity distributions capture the main characteristics of the line profiles. The velocity distributions will therefore be called profiles (or spectra) for simplicity in what follows. A total number of 1.6×10^4 individual spectra are therefore obtained across the face of the

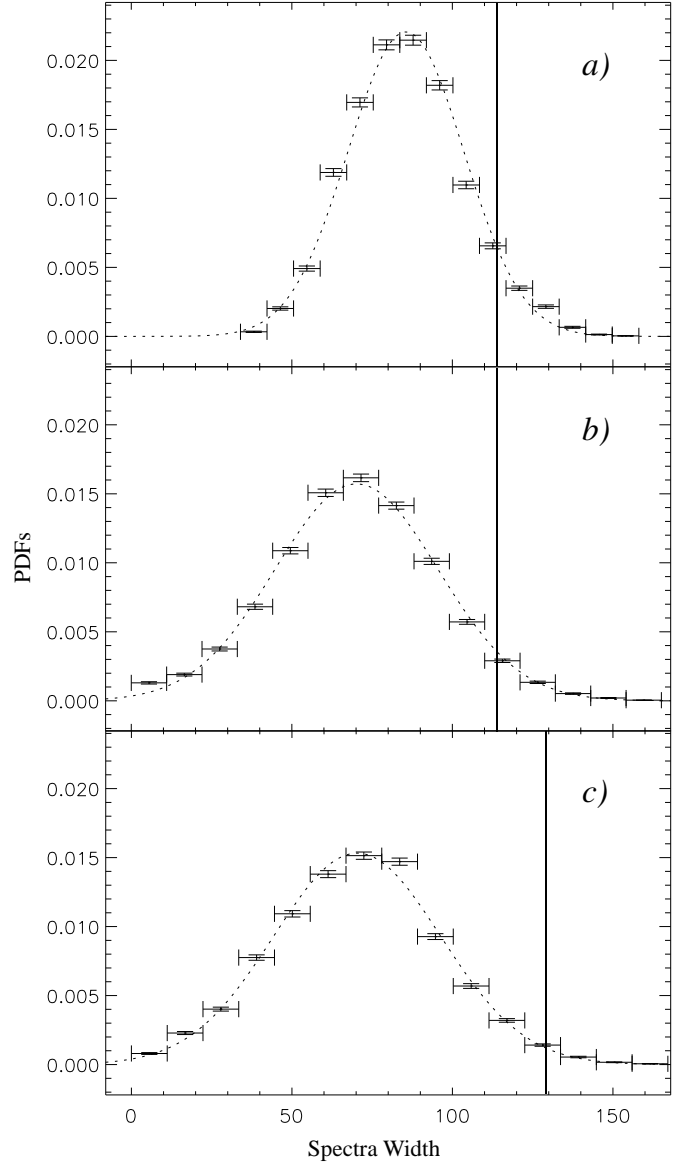


Fig. 3. PDFs of the velocity widths of the 1.6×10^4 individual spectra, each sampling $4 \times 4 \times 512$ pixels, and therefore mimicking spectra obtained with a beam 128 times narrower than that obtained by integrating the emission of the whole cube. The spectra are built on (a) the complete velocity field, and on only 3% of the data points selected (b) as the most intense vortices and (c) as the most intense shocks. The vertical bar, in each panel indicates the width, at the same level, of the integrated spectrum over the whole cube.

cube, for each set. To achieve the comparison of these individual spectra (surrogates of pencil beam spectra) with the total spectrum (surrogate of the large beam spectrum), we use a width computed at levels 1%, 8%, 16% and 32% of the local peak of the velocity distribution (spectrum). Radiative transfer affects more severely the velocity domains where the crowding is the largest (the peaks of the velocity distributions) and this is the reason why we analyze the velocity coverage of each

Table 1. Comparison of integrated and individual spectra.

Sample	level	Integrated spectrum		Individual spectra		
		f_v	Δv_{tot}	f'_v	Δv_{mp}	$\frac{\Delta v_{\text{tot}} - \Delta v_{\text{mp}}}{\Delta v_{\text{tot}}}$
full field	8%	1	114	6×10^{-5}	85	0.25
	16%		97		73	0.25
large ω	8%	3×10^{-2}	113	2×10^{-6}	70	0.38
	16%		96		64	0.33
large $ \nabla \cdot v $	8%	3×10^{-2}	130	2×10^{-6}	70	0.46
	16%		110		62	0.44

distribution at levels low enough for radiation to be reasonably assumed optically thin.

We have computed the probability distribution functions (PDF) of the widths of the individual profiles at the four levels quoted above. They are shown on Fig. 3 at the 8% level for the whole velocity field and the large vorticity and divergence subsets. The dotted curve shows the Gaussian distributions with the same mean and dispersion. On each panel, the vertical bar indicates the width of the large beam profile at the same level (Δv_{tot} in Table 1). The width (Δv_{PDF}) and peak (i.e. most probable value, Δv_{mp}) of the PDFs are given in Table 1 for the 8% and 16% levels and differ by less than 20% with the level selected. The volume filling factors f_v and f'_v represent the fraction of points included in each sample.

In all cases, the pencil beam spectra are narrower than the large beam spectrum but by only 25 to 45% (column 7 of Table 1) while the projected sizes of the sampled volumes differ by a factor 128. This is due to the fact that although the projected size of the volumes sampled by the pencil beams are small, the depth along the line of sight has remained unchanged (512). Along one dimension at least, the pencil beam samples the velocity over large scales. We have made similar computations for $8 \times 8 \times 512$ and $32 \times 32 \times 512$ pencil beams and the widths of the corresponding velocity distributions remain almost the same. For this reason we believe that the results for a pencil beam as small as those of actual observations compared to the large beam (i.e. $60''/0.001'' = 6 \times 10^4$, a ratio which cannot be achieved by any direct numerical simulation) would not be significantly different. As long as the depth of the medium sampled by the line of sight is large, the velocity signature of the pencil beam profile remains close to that of these large scales.

Then it is interesting to note that the differences between the subsets of strong shocks and intense vortices are not marked. On average, vortices produce pencil beam profiles closer to the large beam profile than do the shocks, but the effect in the present simulation is small.

2.3. PDFs of line centroid increments

We have computed the line centroid of each spectrum across the face of the cube according to the method described in Lis et al. (1996). Fig. 2.3 displays the probability distribution functions of the transverse increments of these centroids for several lags. These PDFs are normalized to the rms dispersion of the increments. The comparison of the PDFs obtained for the full velocity field (Fig. 2.3a) with those obtained with the 3% most intense vortices (Fig. 2.3b) and shocks (Fig. 2.3c) shows that, at the smallest lag, the non-Gaussian tails of the PDFs extend much further for the latter subsets than for the former. Non-Gaussian tails disappear at $\Delta = 9$ for the full velocity field while they persist up to $\Delta = 15$ for the regions of large divergence and large vorticity. The non-Gaussian tails of the PDFs of line centroid increments have been shown to be associated with regions of enhanced vorticity in turbulence (Lis et al., 1996). This result shows that both the subsets of shocks and vortices exhibit pronounced non-Gaussian behaviour in those PDFs.

3. Spatial distribution of the high vorticity/divergence subsets

3.1. Channel maps

The three channel maps of Fig. 5 display the surface filling factor of the data points in five adjacent velocity intervals for the whole cube and the two subsets of vortices and shocks. To optimize the visibility of the weakly populated regions, the color scale does not span the whole dynamic range and is not the same in each velocity interval. At almost all velocities, the surface filling factors reach larger values for the shocks than for the vortices (see caption of Fig. 5). Thus the shocks are more clustered in space than the vortices. Shocks also appear as thicker (or more extended) projected structures than vortices. Both subsets have a much more pronounced filamentary texture than the whole velocity field. Many small scale filaments are visible with lengths reaching a significant fraction of the integral scale. This result has been already recognized for the regions of large vorticity by Vincent & Meneguzzi (1991; 1994) or She, Jackson & Orszag (1990) in incompressible turbulence

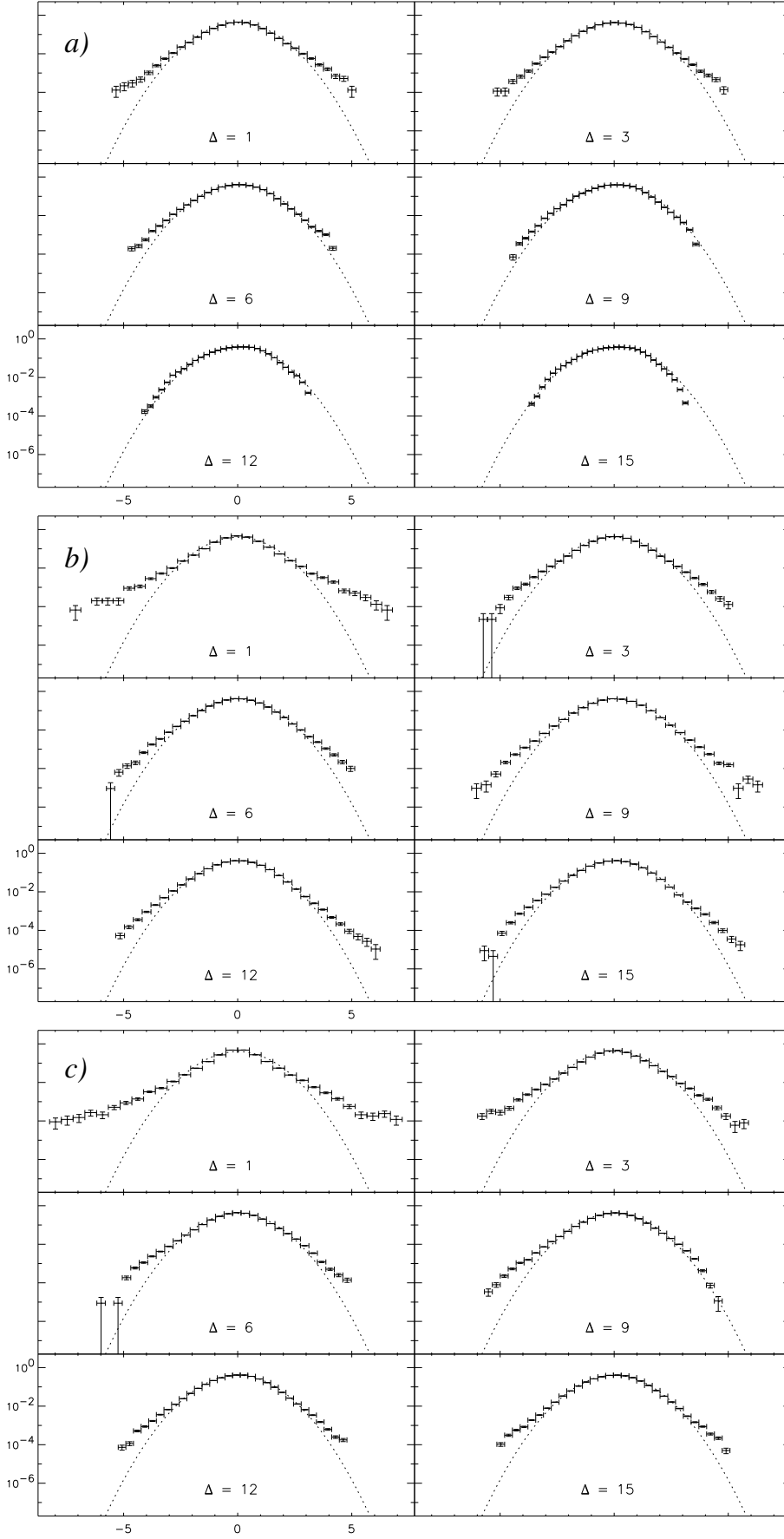


Fig. 4. PDFs of the line centroid increments for different lags Δ and (a) the full velocity field, (b) the subset of most intense vortices and (c) the subset of positions of largest negative divergence.

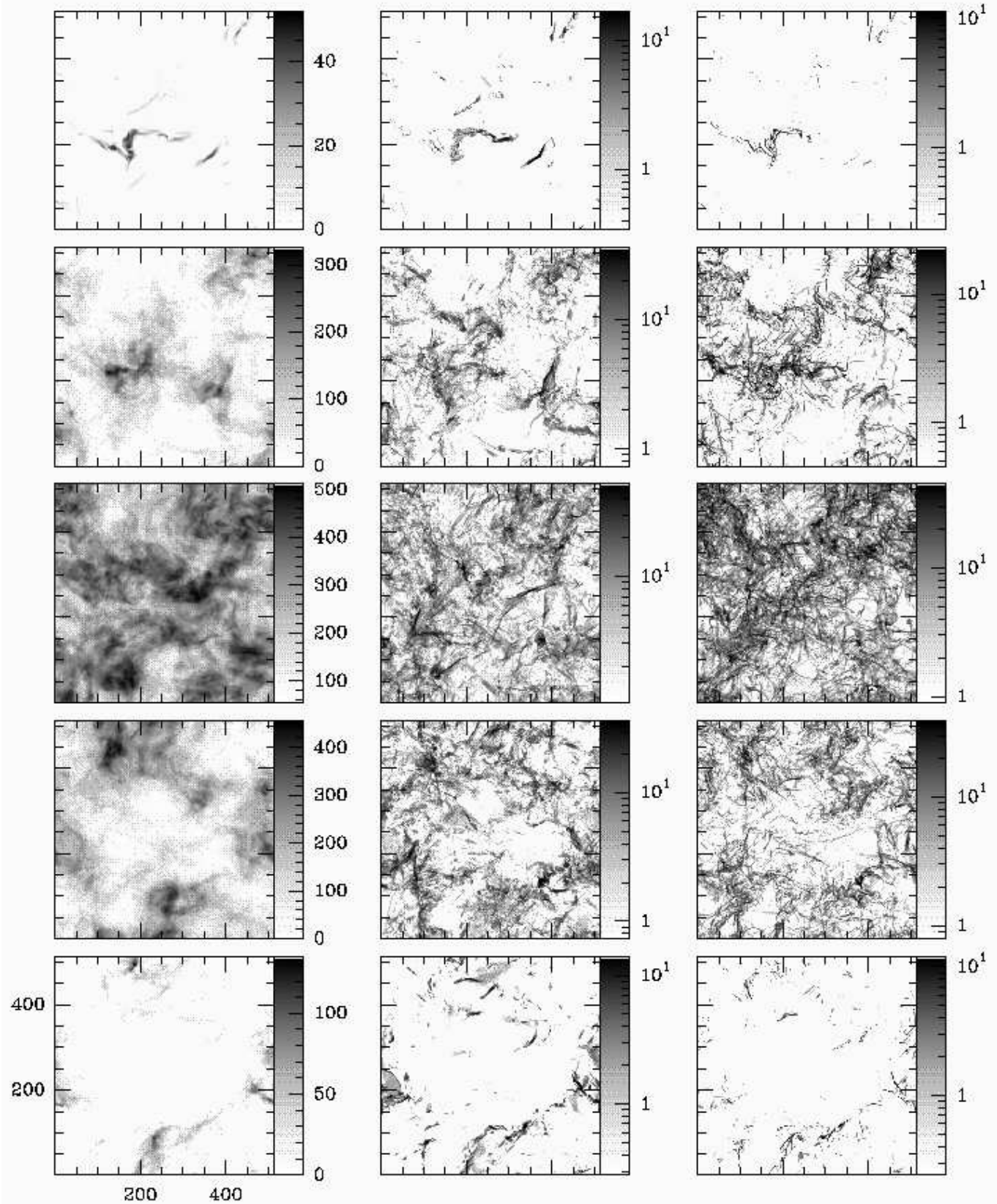


Fig. 5. Channel maps of the surface filling factor on each line of sight in (a) the complete velocity field, (b) the subset of the most intense vortices and (c) the subset of the largest negative divergence. The color scales are different for each velocity range and do not cover the whole dynamic range for the vortices and the shocks. From top to bottom panel, the values of the actual maxima are (52, 326, 512, 457, 135) for the complete velocity field, (23, 46, 90, 79, 24) for the vortices and (36, 83, 116, 73, 30) for the shocks.

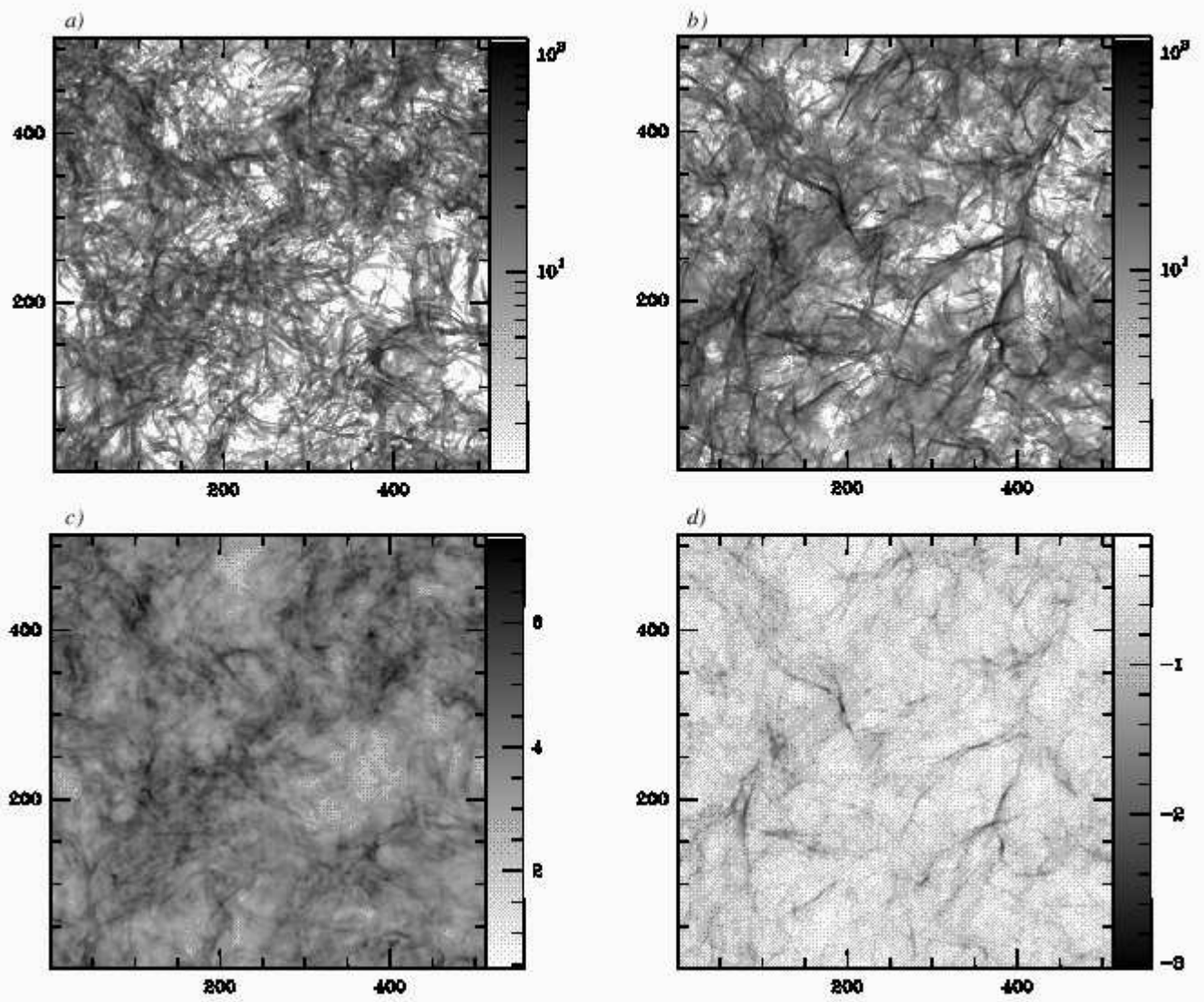


Fig. 6. Maps of the surface filling factors of (a) the most intense vortices (b) the regions of largest negative divergence. Maps of line-of-sight average of (c) the vorticity modulus and (d) the negative divergence.

and by Porter, Woodward & Pouquet (1998) in compressible turbulence.

For the bulk of the structures, there is no coincidence between the patterns delineated by the shocks and the vortices. There are exceptions, though, like the structures seen in the extreme velocity channels. The small scale patterns delineated in these channels by the regions of large vorticity or large divergence closely follow each other, although the details do not exactly coincide. It is remarkable that all the small scale patterns seen in the extreme velocity channels in the maps of large vorticity and divergence are also those of the full velocity field (Fig. 5a): in the first channel (top left), the data points of the full velocity field are either shocks or vortices or both.

These maps also show that shocks and vortices are not randomly distributed but are clustered in space and in velocity. There are large voids with only a few vortex or shocks on the

line of sight. The contrasts are large as indicated by the peak values given in the caption of Fig. 5.

3.2. Integrated maps and surface filling factors

We now turn to the spatial distribution across the face of the cube of the two subsets of shocks and vortices. The set of randomly selected positions does not have any significant spatial structure. It is therefore not shown. The spatial distribution of the surface filling factor f_s is shown in Fig. 6 for the vortices and the shocks.

Fig. 6 shows that the contrasts are large ($\approx 100 : 1$) in the two subsets for which the average surface filling factor per pixel is only 15.3 (i.e. 3% of the data points over 512^2 pixels). There are only 5% and 2% empty lines of sight for the vortices and the shocks respectively, i.e. the surface filling factors of the

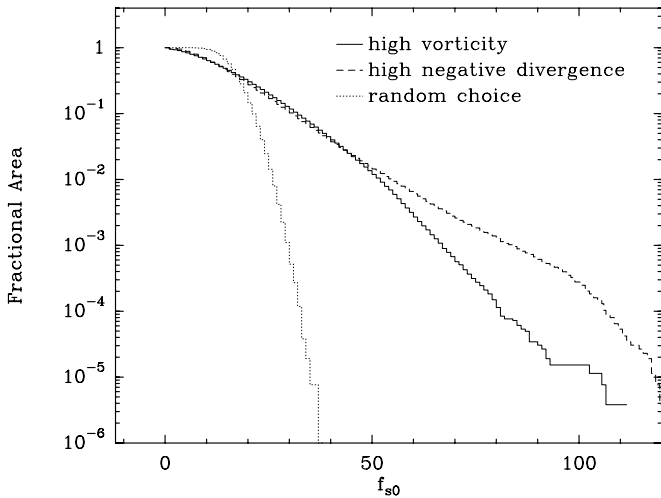


Fig. 7. Fractional area covered by the structures with a surface filling factor above a threshold f_{s0} in the high vorticity (solid) and high negative divergence (dashed) subsets. The same curve for the randomly selected positions is the dotted curve.

regions of large vorticity or large divergence are almost everywhere larger than unity, although they fill only 3% of the whole volume. These numbers depend on the thresholds selected for the vorticity and divergence.

The maps of the filling factors (Figs. 6a and 6b) are very similar to the maps of the vorticity and of the negative divergence (Figs. 6c and 6d) computed with the whole data cube. In particular the maxima in vorticity and in negative divergence are those of the surface filling factors of the upper tails of the corresponding distribution. It means that for the vortices and for the shocks, the origin of the maxima observed in projection is the crowding of rare events populating the upper tails of the distributions.

We have computed the fractional area covered by structures with surface filling factors larger than a threshold f_{s0} . The dependence of this fractional area on f_{s0} is shown in Fig. 7. Unlike randomly selected positions (dotted curve), the high vorticity/divergence distributions exhibit structures with large filling factors which cover only a tiny fraction of the total area. The large crowdings of shocks are more numerous than those of vortices, but the bulk of the ensemble of vortices (those which fill most of the surface, $f_{s0} < 50$) cover a fractional area slightly larger than the bulk of the shocks.

4. Comparison with observations

Statistics on molecular absorption lines in the cold diffuse medium are still sparse. We have used the data set of Liszt & Lucas (1998) to compare the velocity widths of 9 pairs of $^{13}\text{CO}(1-0)$ and $^{13}\text{CO}(2-1)$ absorption and emission lines toward extragalactic sources. In 5 cases (B1730, B2013, B2200 and B2251), the ^{12}CO lines are simple enough that a comparison between the emission and absorption profiles is meaningful. Out of the 14 pairs, two exhibit emission and absorption

profiles of equal widths, three have absorption profiles larger than the emission profiles (this is a possible configuration according to the simulations, see Fig. 3) and nine have absorption narrower than emission profiles. The differences are not large and the average value of the 9 relative width differences ($\Delta v_{\text{em}} - \Delta v_{\text{abs}} / \Delta v_{\text{em}}$) is only 0.34. This number is very close to the values listed in Column 7 of Table 1 for the subset of large vortices (although the difference with that of large divergence is not significant).

Another interesting property of the molecular line absorption measurements is the large scatter of column densities detected for a given amount of gas sampled by the line of sight, N_{tot} . On average, the observed column density of CH^+ for instance increases almost linearly with N_{tot} (see references in Joulain et al. (1998)), but the scatter of the values at a given value of N_{tot} is large. Scatters of about a factor 10 are found in merging the samples of Crane et al. (1995) and Gredel (1997). It means that the spatial distribution of the structures bearing these molecules is highly heterogeneous, although *on average*, the larger the total column density of gas sampled, the larger the column density of molecules. This characteristic may be brought together with the fact that the surface filling factor of the most intense vortices and shocks have large fluctuations (a factor ~ 10) about their average value (15) (Figs. 6a and 6b).

5. Conclusion

The regions of largest vorticity or largest divergence in compressible turbulence are small subsets of a whole turbulent velocity field but we have shown that, despite their small volume filling factor (here $f_v = 0.03$):

- (i) they sample the whole velocity field,
- (ii) pencil beam samplings across these subsets have velocity coverages almost as broad as those obtained with large beams. The values (35% to 45%) and the signs of these differences are consistent with the observations.
- (iii) the PDFs of centroid velocity increments built on these subsets have more extended non-Gaussian wings than those of the full velocity field. Their intermittent characteristics subsist at larger lags than for the full velocity field.
- (iv) copious small scale structure with large contrasts is seen in the maps of the surface filling factor of the regions of large vorticity and large divergence. These contrasts are of the same order of magnitude as those observed in the column densities of CH^+ for instance for a given column density of sampled gas.
- (v) the surface filling factor of the subsets of high vorticity/divergence are almost everywhere larger than unity even though their volume filling factor is as small as 3% in the subsets studied here. Vortices are slightly more efficient than shocks at covering the sky: they tend to be more numerous, and to form smaller structures which are less clustered in space.

In summary our study confirms that mild shocks as well as intense vortices could be the subsets of the cold diffuse medium enriched in molecules and responsible for the molecular absorption lines detected in the direction of extragalactic sources.

Numerical simulations of hydrodynamical turbulence are not ideally suited to test the properties of such subsets, but one-fluid simulations of MHD turbulence are not ideal either because of the importance of the ion-neutral streaming in the triggering of hot chemistry, whether in MHD shocks or in magnetized vortices. More detailed predictions of the phase-space structures of the subsets of turbulence where hot chemistry is activated in the cold diffuse medium require calculations of MHD compressible turbulence which take ion-neutral drift into account.

Acknowledgements. We thank D. H. Porter, A. Pouquet, and P. R. Woodward for providing us with the result of their hydrodynamic simulation and our referee, A. Lazarian, for his helpful comments.

References

Brandenburg, A., Jennings, R. L., Nordlund, A. K., Rieutord, M., Stein, R. F., and Tuominen, I., 1996, *J. Fluid Mech.* 306, 325

Crane, P., Lambert, D. L., and Sheffer, Y., 1995, *ApJS* 99(1), 107

Draine, B. T., 1986, *ApJ* 310(1), 408

Draine, B. T. and Katz, N., 1986, *ApJ* 310(1), 392

Elitzur, M. and Watson, W. D., 1978, *ApJ Lett.* 222, L141

Falgarone, E., Lis, D. C., Phillips, T. G., Pouquet, A., Porter, D. H., and Woodward, P. R., 1994, *ApJ* 436(1), 728

Falgarone, E., Pineau des Forts, G., and Roueff, E., 1995, *A&A* 300(3), 870

Falgarone, E. and Puget, J.-L., 1995, *A&A* 293(3), 840

Flower, D. R. and Pineau des Forts, G., 1995, *MNRAS* 275(4), 1049

Flower, D. R. and Pineau des Forts, G., 1998, *MNRAS* 297(4), 1182

Galtier, S., Gomez, T., Politano, H., and Pouquet, A., 1998, in U. Frisch (ed.), *Advances in Turbulence VII*, pp 453–456, Kluwer Academic Publishing

Goldreich, P. and Sridhar, S., 1995, *ApJ* 438(2), 763

Gredel, R., 1997, *A&A* 320(3), 929

Joulain, K., Falgarone, E., Pineau des Forts, G., and Flower, D., 1998, *A&A* 340(1), 241

Lazarian, A. and Vishniac, E. T., 1999, *ApJ* 517(2), 700

Lis, D. C., Pety, J., Phillips, T. G., and Falgarone, E., 1996, *ApJ* 463(1), 623

Liszt, H. S. and Lucas, R., 1994, *ApJ Lett.* 431(2), L131

Liszt, H. S. and Lucas, R., 1995, *A&A* 294(3), 811

Liszt, H. S. and Lucas, R., 1998, *A&A* 339(2), 561

Lucas, R. and Liszt, H. S., 1993, *A&A* 276(1), L33

Lucas, R. and Liszt, H. S., 1994, *A&A* 282(1), L5

Lucas, R. and Liszt, H. S., 1996, *A&A* 307(1), 237

Lucas, R. and Liszt, H. S., 1997, in E. F. Van Dishoeck (ed.), *Molecules in Astrophysics: Probes and Processes*, Vol. 178 of IAU Symposium, pp 421–430, Kluwer Academic Publisher, Leiden

Ostriker, E. C., Gammie, C. F., and Stone, J. M., 1999, *ApJ* 513(1), 259

Pineau des Forts, G., Flower, D. R., Hartquist, T. W., and Dalgarno, A., 1986, *MNRAS* 220(4), 801

Politano, H. and Pouquet, A., 1995, *Phys. Rev. E* 52(1), 636

Politano, H. and Pouquet, A., 1998a, *Geophys. Res. Lett.* 25(3), 273

Politano, H. and Pouquet, A., 1998b, *Phys. Rev. E* 57(1), R21

Porter, D. H., Pouquet, A., and Woodward, P. R., 1994, *Phys. Fluids* 6(6), 2133

Porter, D. H., Woodward, P. R., and Pouquet, A., 1998, *Phys. Fluids* 10(1), 237

She, Z. S., Jackson, E., and Orszag, S. A., 1990, *Nat* 334, 226

Tabeling, P., Zocchi, G., Belin, F., Maurer, J., and Willaime, H., 1996, *Phys. Rev. E* 53(2), 1613

Verstraete, L., Falgarone, E., Pineau des Forts, G., Flower, D., and Puget, J.-L., 1999, in P. Cox and M. F. Kessler (eds.), *The Universe as Seen by ISO*, Vol. 2, pp 779–782, ESA, UNESCO, Paris

Vincent, A. and Meneguzzi, M., 1991, *J. Fluid Mech.* 225, 1

Vincent, A. and Meneguzzi, M., 1994, *J. Fluid Mech.* 258, 245

Wiklind, T. and Combes, F., 1997, *A&A* 328(1), 48

Wiklind, T. and Combes, F., 1998, *ApJ* 500(1), 129